



Depth and Spatial Variation of the Shear Wave Attenuation Parameters in the Shallow Crust and Lower Crust/Upper Mantle of Mt. Etna (Italy)

ELISABETTA GIAMPICCOLO,¹  TIZIANA TUVÈ,¹  FRANCESCA BIANCO,²  and EDOARDO DEL PEZZO^{2,3} 

Abstract—Seismic wave attenuation is a key feature of seismic wave propagation that provides constraints on the composition and physical state of the medium within the Earth. We separated intrinsic and scattering attenuation coefficients for the shallow crust and lower crust/upper mantle in the Mt. Etna area. For this purpose, the Multiple Lapse Time Window Analysis (MLTWA) was applied to two groups of earthquakes, well separated in depth. We also studied the spatial variation of the attenuation parameters by dividing the study area into four sectors around Etna. The results show an effective homogeneity of the propagation characteristics inside Etna and, in particular, some lateral variations and minor variations with depth. We observe that structural discontinuities and lithology control scattering losses at all frequencies, with higher scattering in the shallow crust. The intrinsic absorption shows no sensitivity to the presence of these main geological structures and is quite uniform for different depths. Furthermore, compared to the northern sector of the volcano, the southern one shows stronger scattering attenuation at low frequencies. This pattern correlates well with the high seismic activity along most of Etna's active tectonic structures and ascending magmatic fluids that characterize this sector of the volcano. Although we only discuss the differences in the “average” scattering and inelastic properties of the investigated volumes, the results of this study are very informative about the characteristics of each region. Moreover, they suggest that a future study is necessary, providing a more detailed picture of the spatial distribution of seismic attenuation in the study area, through a 3D inversion of the attenuation parameters estimated along the single source-receiver paths.

Keywords: Seismic attenuation, scattering and intrinsic absorption, coda waves, mt. Etna.

1. Introduction

The structural complexity of volcanoes is a very important factor in controlling the attenuation of seismic energy, covering a wide variety of cases associated with different geological conditions and volcanism (e.g. Del Pezzo, 2008; Sato et al., 2012). Seismic wave attenuation is defined as the decay coefficient of wave amplitude (or Energy) with distance. The total seismic attenuation takes into account the intrinsic absorption (the seismic energy that heats the rock) and the dispersion due to scattering (the diffused energy produced by the spatial fluctuations of the elastic parameters). Conceptually, the intrinsic attenuation coefficient is a measure of the rheology of the rocks, while the scattering coefficient describes the geological heterogeneity. Both effects are present in volcanoes, where the seismic energy can be attenuated by the presence of fluids (both magmatic and hydrothermal) and by the high geological heterogeneity (presence of magmatic packets, multiple stratifications, strong lateral velocity variations). It is therefore essential to correctly estimate the amount of intrinsic dissipation versus scattering attenuation to better understand the volcanic structure and related processes. The attenuation phenomena concern both compression and shear waves. As known, however, shear waves are more sensitive to the presence of fluids and carry the greatest amount of seismic energy. For this reason, we will deal exclusively with shear wave energy.

The depth dependence of both intrinsic and scattering attenuation parameters has been widely observed and reported in the literature (e.g. Badi et al., 2009; Bianco et al., 2002, 2005; Castro-Melgar et al., 2021; Gabrielli et al., 2022; Mayor et al., 2016

Supplementary Information The online version contains supplementary material available at <https://doi.org/10.1007/s00024-023-03400-0>.

¹ INGV Osservatorio Etneo, Piazza Roma 2, Catania, Italy.
E-mail: elisabetta.giampiccolo@ingv.it

² Osservatorio Vesuviano, Via Diocleziano, 328, 80124 Naples, Italy.

³ Andalusian Institute of Geophysics, University of Granada, 18071 Granada, Spain.

and references therein). In these studies, events covering a wide range of focal depths (in some cases focal depths greater than 200 km) were analyzed to estimate the seismic attenuation coefficients, concluding that the depth dependence of seismic attenuation (both intrinsic and scattering) is due to changes in the physical properties of the medium with increasing lithostatic pressure, which in turn strengthens the stiffness of the rock down to the depth of Moho and, at the same time, reduces heterogeneity.

A widely used technique is the so-called MLTWA (Multiple Lapse Time Window Analysis) based on the solution of the Energy Transport Equation (ETE, Paasschens, 1997), which describes the spatial–temporal trend of the Energy Envelope seismogram (Sato et al., 2012), under the simple assumption of constant velocity in half space. The model is parameterized in terms of η_i and η_s , the intrinsic attenuation and scattering coefficients, respectively. The technique is based on the fit of the observed quantities obtained by integrating the energy envelopes of the seismogram with respect to time in three successive time windows with theoretical quantities by applying the same integrals to the ETE. Although more recent techniques based on full envelope inversion are available (van Lateen et al., 2021), MLTWA has been shown to be equivalent for inverting attenuation parameters. Furthermore, we preferred MLTWA to compare our results with previous ones obtained using the same technique. MLTWA will be described in Sect. 4.

In the present work, we measure seismic attenuation in earth volumes located at different depths. For this reason, we estimate the attenuation coefficients $\eta_i = 2\pi f Q_i^{-1}$ and $\eta_s = 2\pi f Q_s^{-1}$ (Q_i and Q_s are, respectively, the intrinsic and scattering quality factors and f is the frequency) by separately analyzing two groups of earthquakes with sources localized in the first 15 km and between 15 and 40 km in the lower crust/upper mantle under Mt. Etna (Fig. 1). Furthermore, differences in the seismic waves velocity observed in the Etna area (De Gori et al., 2021 and references therein), prompted us to perform a more detailed analysis aimed at estimating the attenuation parameters in different sectors of the volcano, dividing the area under study into 4 quadrants, centered on the Etna volcano craters (Fig. 1).

Our main aim was to quantify the possible spatial and depth variation of the Shear Wave attenuation parameters, to improve attenuation studies already published for the Etna area (briefly described in Sect. 3) that report parameters space-averaged for the whole Etna volume (a crustal average of η_i and η_s). The current availability of high-quality seismograms from local shallow ($h \leq 5$ km), intermediate ($5 \text{ km} > h \leq 15$ km) and deep ($h > 15$ km) earthquakes with $M_L \geq 1.0$ recorded since 2006 by the permanent seismic network of the Istituto Nazionale di Geofisica e Vulcanologia (INGV-OE) allowed us to: i) refine previously deduced attenuation estimates for the shallow crust (Del Pezzo et al., 2015, 2019, see next section), thanks also to the high number of shallow earthquakes recorded during the last flank eruption which took place on December 24, 2018; ii) evaluate, for the first time, the attenuation characteristics for the lower crust/upper mantle, using data from deeper sources. The new data set was also used in the present work to verify the Q-coda (Q_c) results recently obtained in the same area by Giampiccolo et al., (2021) using a different dataset.

2. Geological and Geophysical Framework of the Mt. Etna Area

Mt. Etna, is a Quaternary active stratovolcano, with an elevation of about 3300 m above sea level, located on the east coast of Sicily on the front of the Apennine-Maghrebic collision belt (Lentini, 1982) and on the flexured margin of the Hyblean plateau (Branca et al., 2008; Monaco et al., 2010). The Etna's area tectonic setting is the result of a complex interaction between regional stress, dike-induced rifting and gravitational forces (Lo Giudice & Rasà, 1992; Monaco et al., 1997). The regional deformation is dominated by N-S active compression in the northern sector, (Bousquet & Lanzafame, 2004). This regime coexists with active E-W extension on the eastern flank and with right-lateral transtension both onshore along the Timpe Fault System (TFS; Fig. 1a), a set of parallel normal faults with NW–SE and NNW–SSE directions (Azzaro et al., 2012), and offshore along the Malta Escarpment Fault System (MEFS; inset in Fig. 1a). The volcanic edifice is also affected by

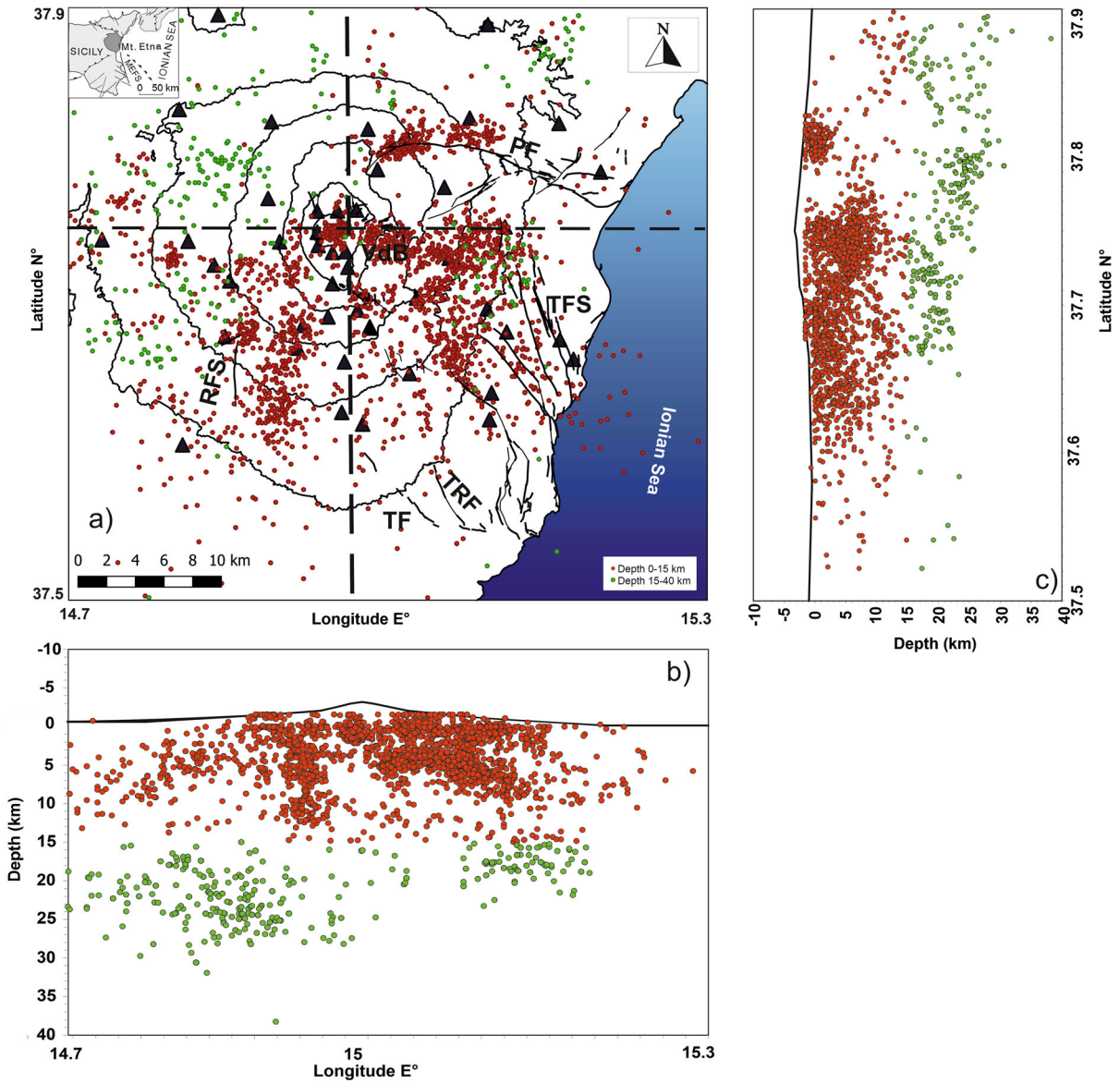


Figure 1

a Map of the Mt. Etna volcano and main tectonic elements. The seismic stations of the INGV-OE network are indicated with black triangles, shallow seismicity ($h \leq 15$ km) with red dots and deep seismicity ($15 < h \leq 40$ km) with green dots. **b**, **c** W-E and S-N sections crossing the summit craters along the profiles (dashed black lines) shown in **a**

deformations related to the volcano dynamics (inflation and deflation), volcano-tectonic processes, such as ground fracturing induced by dike intrusion in the summit area, and regional faulting and instability in the eastern flank (Azzaro et al., 2013).

The seismicity of Mt. Etna is characterized by volcano-tectonic earthquakes (VT; Patanè et al., 2004 and reference therein) mainly occurring in the shallow crust ($h < 10$ km). The most seismically active area is the eastern flank of the volcano, mainly along

the TFS (Fig. 1a). Other seismogenic structures are the Pernicana Fault with E-W trend (PF; Fig. 1a) in the northeastern sector, the Ragalna Fault System with N-S trend (RFS; Fig. 1a) and the Tremestieri and Trecastragni faults with NW–SE trend (TF; TRF Fig. 1a) in the southern one (Alparone et al., 2013; Azzaro et al., 2013 and references therein). The activity of these structures generates frequent VT earthquakes which, although of moderate magnitude, can cause serious damage and destruction. Intermediate-depth events ($10 \leq h \leq 15$ km) are expected mainly on the western flank while deep seismicity ($15 \leq h \leq 35$ km) is mostly confined to the north-western sector of the volcano (Fig. 1; Sicali et al., 2014 and references therein).

3. Previous Attenuation Measurements at Mt. Etna

A comprehensive review of the body wave seismic attenuation at Mt. Etna was produced by Del Pezzo et al. (2015), hereinafter referred to as DP15. These authors report the measurements described in four articles: Patané et al. (1994), hereinafter referred to as PA94; Del Pezzo et al. (1995), hereinafter referred to as DP95; de Lorenzo et al. (2006), hereinafter referred to as DL04; and Giampiccolo et al. (2007), hereinafter referred to as GP07. In the above studies, the attenuation measurements were performed using different techniques, mentioned in DP15 and described in the appendix of DP15. A summary of these results is shown in Fig. 1 and Table 2 of DP15. DP15 also uses the MLTWA technique (see Sect. 3 for a brief description) to check the stability and robustness of the previous estimates by fitting the data with a more general and suitable model.

More recently, Del Pezzo et al. (2019), hereinafter DP19, estimated intrinsic and scattering attenuation coefficients using a slightly modified version of MLTWA (see Appendix A of the present paper) for the shallow crust of the whole Sicily (above 20 km), including both volcanic and tectonic regions. The results obtained from DP15 and DP19 are shown in

Table 1

Estimates of Q_i^{-1} , Q_s^{-1} and Q_t^{-1} obtained in previous seismic attenuation studies at Mt. Etna

| f (Hz) | Q_i^{-1} | Q_s^{-1} | Q_t^{-1} | Dist. range (km) | Method |
|--------|------------|------------|------------|------------------|-------------|
| 1.5 | 0.0069 | 0.0625 | 0.0714 | 0–20 | MLTWA(DP15) |
| 3.0 | 0.0056 | 0.0263 | 0.0323 | 0–20 | MLTWA(DP15) |
| 6.0 | 0.0038 | 0.0053 | 0.0091 | 0–20 | MLTWA(DP15) |
| 12.0 | 0.0012 | 0.0004 | 0.0016 | 0–20 | MLTWA(DP15) |
| 1.5 | 0.0064 | 0.0192 | 0.0256 | 0–50 | MLTWA(DP15) |
| 3.0 | 0.0053 | 0.0079 | 0.0133 | 0–50 | MLTWA(DP15) |
| 6.0 | 0.0038 | 0.0034 | 0.0071 | 0–50 | MLTWA(DP15) |
| 12.0 | 0.0012 | 0.0004 | 0.0016 | 0–50 | MLTWA(DP15) |
| 1.5 | 0.0062 | 0.0303 | 0.0370 | 0–50 | MLTWA(DP15) |
| 3.0 | 0.0052 | 0.0125 | 0.0179 | 0–50 | MLTWA(DP15) |
| 6.0 | 0.0038 | 0.0041 | 0.0079 | 0–50 | MLTWA(DP15) |
| 12.0 | 0.0012 | 0.0004 | 0.0016 | 0–50 | MLTWA(DP15) |
| 1.0 | 0.0263 | 0.0053 | 0.0313 | 0–50 | W93(DP15) |
| 2.0 | 0.0159 | 0.0063 | 0.0222 | 0–50 | W93(DP15) |
| 4.0 | 0.0095 | 0.0061 | 0.0156 | 0–50 | W93(DP15) |
| 8.0 | 0.0056 | 0.0054 | 0.0111 | 0–50 | W93(DP15) |
| 12.0 | 0.0042 | 0.0049 | 0.0090 | 0–50 | W93(DP15) |
| 18.0 | 0.0031 | 0.0043 | 0.0074 | 0–50 | W93(DP15) |
| 1.5 | 0.0060 | 0.0179 | 0.0238 | 0–50 | MLTWA(DP19) |
| 3 | 0.0050 | 0.0092 | 0.0141 | 0–50 | MLTWA(DP19) |
| 6 | 0.0037 | 0.0045 | 0.0082 | 0–50 | MLTWA(DP19) |
| 12 | 0.0012 | 0.0003 | 0.0012 | 0–50 | MLTWA(DP19) |

Table 1. Despite the number of published papers, there are still no studies on seismic wave attenuation in the lower crust/upper mantle. Furthermore, no attempt has been made so far to investigate possible spatial variations of seismic attenuation in terms of intrinsic absorption and scattering inside the Etna volcanic complex.

4. MLTWA Technique

Introduced by Fehler et al. (1992), this technique has been widely applied in the literature to discriminate between scattering and intrinsic attenuation in both tectonic areas and volcanoes (Akinci et al., 2020; Badi et al., 2009; Del Pezzo et al., 2019; Hoshiba et al., 2001; Mayeda et al., 1992; Sato et al., 2012; Singh et al., 2017). MLTWA is based on the calculation of the integral of the signal energy,

normalized by the energy of the coda waves measured in a time window centered at a lapse time common to the whole data set. This procedure (generally called coda normalization) normalizes all the data for the source's intensity (Aki, 1980). The Energy integral is estimated in three successive time windows along the seismogram, which fit the corresponding Energy integrals derived from the scalar approximation of the Energy Transport Equation solution (ETE, Paasschens, 1997).

The fit yields two attenuation parameters: η_i and η_s . Since Paasschens' solution of ETE can be obtained analytically only assuming uniform velocity, the basic assumption that most researchers make in their applications of MLTWA is the half-space approximation (earth medium with constant velocity), far from being realistic in most experimental cases. This approximation produces a bias in the determination of η_i and η_s , which are slightly underestimated (see Del Pezzo & Bianco, 2010) compared to those based on numerical estimates of ETE in more realistic earth structures. The pair of parameters, η_i and η_s , can be expressed in terms of other quantities: the pair formed by seismic albedo, B_0 and the extinction length, Le^{-1} , or the pair of quality factors Q_i and Q_s . All these parameters are related to each other by the following equations:

$$B_0 = \frac{\eta_s}{\eta_s + \eta_i} = \frac{Q_s^{-1}}{Q_i^{-1} + Q_s^{-1}}; \quad Le^{-1} = \eta_s + \eta_i \\ = \frac{2\pi f}{v} (Q_s^{-1} + Q_i^{-1})$$

Unlike most of the works dealing with the application of the same technique, we have estimated the three Energy Integrals by means of a direct Fourier Transform (FT). Instead, most MLTWA applications use the filtering and averaging procedure to process the seismograms. An appropriate Mathematica™ code (Wolfram Research & Inc., 2022) was used for the analysis. A more detailed description of the MLTWA technique is provided in Appendix A.

5. Data Analysis and Results

We selected from the INGV-OE database 14,440 earthquake data with $M_L \geq 1.0$ recorded at Mt. Etna

from 2006 to 2021 at the seismic stations of the INGV-OE permanent network, equipped with broadband (0.01–40 s) three-component seismometers (see Table S1 in Supplementary Material). Signals are digitized at 100 samples per second with 24-bit resolution at each station. The arrival times of P- and S-waves were read manually on the digital waveforms and the earthquakes location parameters were selected from the INGV-OE catalog (Alparone et al., 2015, 2020a, 2020b, 2022; Barberi et al., 2020). These events have been selected as the best-located ones on the basis of the following criteria: at least 6P and 2S arrival times, root mean squared travel time residual, RMS, of less than 1 s, hypocentral errors ≤ 1.0 km and azimuthal gap ≤ 180 degrees. From the entire dataset, 5734 earthquakes were considered suitable for the attenuation study in the present work (Fig. 1), for a total of 16,285 horizontal EW and NS components waveforms selected on the basis of their quality (average signal-to-noise ratio greater than 5 in a 15 s time window starting at 60 s from the time of origin, absence of multiple signals in the coda, telemetry peaks, and gaps).

5.1. Depth Dependence of Q_i^{-1} , Q_s^{-1} and Q_c^{-1}

To compute Q_i^{-1} and Q_s^{-1} for Etna's shallow crust and lower crust/upper mantle we separately analyzed two groups of events (Fig. 1) located in the depth intervals $0 \leq h \leq 15$ km (4461 earthquakes) and $15 < h \leq 40$ km (1273 earthquakes). Hence, approximately 14,200 and 2,000 horizontal two-component waveforms were considered suitable for the attenuation study in the shallow and deep depth range, respectively. The waveforms were processed as follows: from three consecutive 12-s time windows after S-wave onset (Fig. 2a, b) the integral of energy in four different frequency bands centered at 1.5, 3, 6, and 12 Hz has been estimated by using FT (see DP19 for further details). To correct for the source intensity and site effects, each integral was normalized by the spectral amplitude of the coda (Aki, 1980) averaged over a 12 s window, the center of which was fixed at a reference time (t_c) of 45 s measured from the origin time of each earthquake (Fig. 2a, b). The average velocity V_s of the S wave was set at 3.5 km/s.

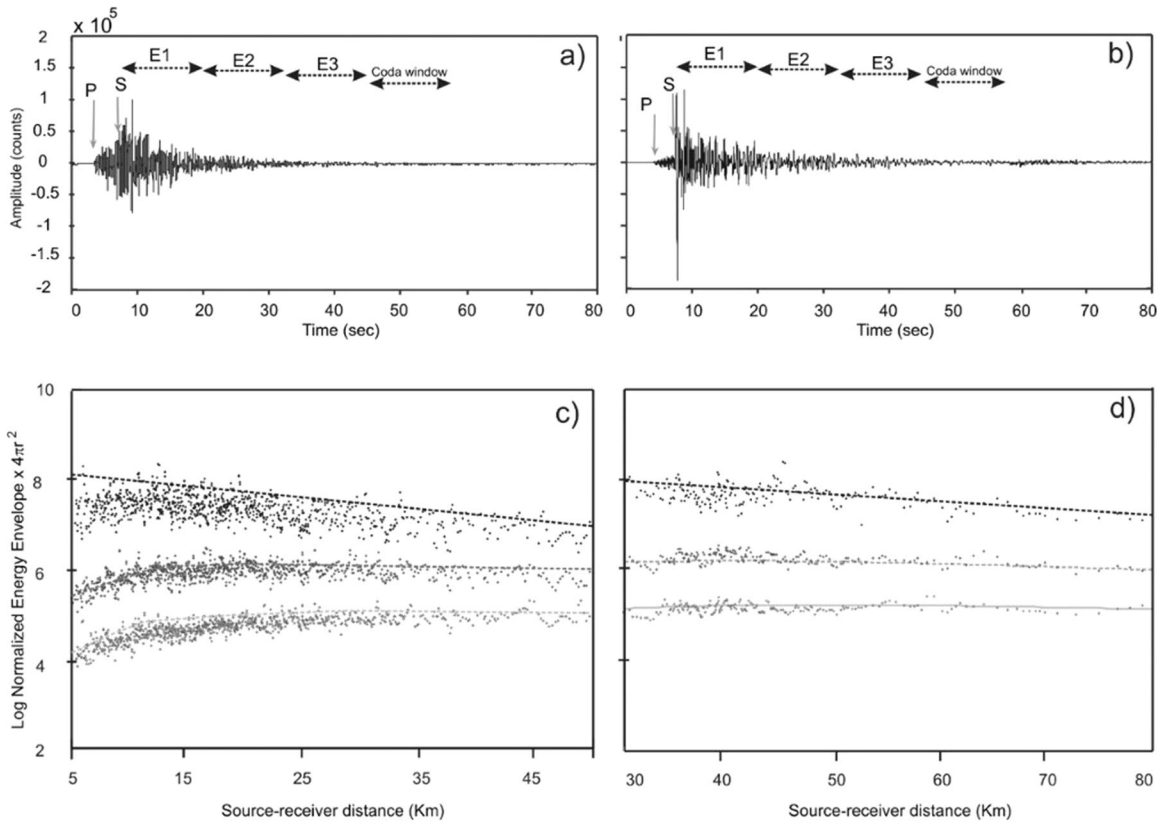


Figure 2

a, b Indicative seismograms, showing the coda shape for a shallow (0–15 km) and deep (15–40 km) earthquake, respectively. The segments marked by E1, E2, and E3 represent the position and duration (0–12, 12–24, and 24–36 s) of the time-windows used for MLTWA. **c, d** Energy Envelope (dots) integrated in the first, second and third window (E1 (black), E2 (dark grey) and E3 (light grey)), normalized by the coda energy integrated in the coda window, all corrected for the geometrical spreading (spherical surface: $4\pi r^2$), and respective theoretical best fit (bold dashed curves) at 3 Hz for shallow and deep earthquakes, respectively

In Fig. 2a and b we plot the seismogram showing the three time windows and the coda window used for the application of MLTWA for a shallow and deep event, respectively. The corresponding integrated energies as a function of distance for the central frequency of 3 Hz, normalized for the coda and corrected for geometrical spreading (see Appendix A for details), are shown in Fig. 2c and d. The fitting of the experimental data to the theoretical curves was carried out in the same way as described by DP19, using a grid search method in the parameter space, where the seismic albedo (B_0) ranges from 0.005 to 0.95, with steps of 0.005, while the inverse of the

extinction length (Le^{-1}) ranges from 0.005 to 0.12, with steps of 0.005. The sum of the residual least squares was normalized for the minimum value, following the procedure described by Mayeda et al., (1992). The uncertainties have been estimated by calculating the area in the coordinates B_0 and Le^{-1} representing the normalized squared residuals that are not statistically different at the 70% confidence level (e.g., Del Pezzo & Bianco, 2010; Del Pezzo et al., 2019). In the case of multiple minima in the residual distribution, the area of uncertainty was assumed as the overall area including the minima, while the pair

Table 2

Measured B_0 and Le^{-1} and the corresponding inverse of the Quality Factors, together with the 1-sigma uncertainties, in each depth range

| Depth | N.W. | f (Hz) | B_0 | Le^{-1} | Q_i^{-1} | Q_s^{-1} | Q_t^{-1} | Q_c^{-1} |
|----------|--------|--------|------------------|-------------------|---------------------|---------------------|---------------------|---------------------|
| 0–15 km | 14,277 | 1.5 | 0.85 ± 0.0 | 0.088 ± 0.002 | 0.0049 ± 0.0 | 0.0278 ± 0.0 | 0.0327 ± 0.0 | 0.0141 ± 0.0042 |
| | | 3 | 0.75 ± 0.025 | 0.104 ± 0.010 | 0.0048 ± 0.0002 | 0.0145 ± 0.0018 | 0.0193 ± 0.0020 | 0.0104 ± 0.0025 |
| | | 6 | 0.55 ± 0.025 | 0.084 ± 0.008 | 0.0035 ± 0.0008 | 0.0043 ± 0.0011 | 0.0078 ± 0.0019 | 0.0069 ± 0.0011 |
| | | 12 | 0.35 ± 0.050 | 0.044 ± 0.004 | 0.0013 ± 0.0002 | 0.0007 ± 0.0001 | 0.0020 ± 0.0003 | 0.0027 ± 0.0001 |
| 15–40 km | 2008 | 1.5 | 0.75 ± 0.025 | 0.060 ± 0.012 | 0.0056 ± 0.0013 | 0.0167 ± 0.0046 | 0.0223 ± 0.0059 | 0.0122 ± 0.0034 |
| | | 3 | 0.55 ± 0.025 | 0.056 ± 0.008 | 0.0047 ± 0.0019 | 0.0057 ± 0.0024 | 0.0104 ± 0.0043 | 0.0108 ± 0.0029 |
| | | 6 | 0.45 ± 0.0 | 0.068 ± 0.0 | 0.0035 ± 0.0 | 0.0028 ± 0.0 | 0.0063 ± 0.0 | 0.0070 ± 0.0012 |
| | | 12 | 0.25 ± 0.025 | 0.036 ± 0.002 | 0.0013 ± 0.0001 | 0.0004 ± 0.0001 | 0.0017 ± 0.0002 | 0.0034 ± 0.0003 |

The number of waveforms used for the inversion in each depth range is also reported (N.W.)

$\{B_0, Le^{-1}\}$ corresponding to the center of the area of uncertainty was assumed as the best estimate.

In Table 2 we report, for each central frequency investigated, the estimates of B_0 and Le^{-1} together with the corresponding intrinsic (Q_i^{-1}), scattering (Q_s^{-1}), and total (Q_t^{-1}) inverse quality factors, for both shallow (0–15 km) and deep (15–40 km) earthquakes. The 1-sigma uncertainty on each estimate is also reported. It is worth noting that for this analysis we did not apply the corrections for an opaque crust over a transparent mantle, as suggested by Del Pezzo and Bianco (2010), but the values reported in Table 2 were obtained assuming a uniform Earth model. This choice was the result of the DP19 which highlighted that at Etna the difference between the not corrected and the corrected values is not significant. As also observed by Del Pezzo et al. (2011) this happens when scattering is strongly dominant (Del Pezzo & Bianco, 2010).

The Pattern of B_0 , Le^{-1} , Q_i^{-1} and Q_s^{-1} and Q_t^{-1} vs. frequency in both depth ranges investigated is shown in Fig. 3a-e.

We observe that for crustal earthquakes (0–15 km) B_0 is greater than 0.5 below 12 Hz and decreases systematically with frequency. This can be interpreted in terms of an important scattering contribution (Q_s^{-1}) below 12 Hz (Fig. 3c). Interestingly, the current results correspond quite well with the Q estimates obtained at Etna by DP19, based on a different set of earthquake data (depth ≤ 20 km), indicating the robustness of the technique used

(Fig. 3a–e; black dashed line). For deep events (15–40 km) B_0 is greater than 0.5 below 6 Hz. Consequently, scattering dominates over intrinsic absorption below this frequency. The B_0 and Le^{-1} values obtained for shallow earthquakes (in red) and deep (in blue), plotted as a function of frequency, are shown in Fig. 3a and b, respectively. In general, as can be clearly deduced from Table 2 and Fig. 3c and d, Q_i^{-1} is homogeneous at both depth ranges while Q_s^{-1} in the shallow crust is higher at all frequencies. This shows that the contribution of scattering to the total attenuation (Q_t^{-1}) in the shallow crust is very important.

The Q_i^{-1} , Q_s^{-1} Q_t^{-1} values were compared with the Q_c^{-1} estimates obtained from the present data set. For this purpose, we divided the data into two depth ranges, as for MLTWA, and estimated Q_c^{-1} at the same frequency bands for a fixed lapse time (t_c) of 45 s to ensure that the region sampled by the coda envelope is the same as that analyzed in MLTWA. The method used is well described in Giampiccolo et al., (2021). A short description is also reported in Appendix B. The Q_c^{-1} values in each depth and frequency range, obtained by averaging all the values with an uncertainty of less than 40% are reported in Table 2. The pattern of Q_c^{-1} vs. frequency is shown in Fig. 3f. It is remarkable that very similar Q_c^{-1} values were found in the two depth ranges. Moreover, the Q_c^{-1} pattern vs. frequency is comparable with that one of Giampiccolo et al., (2021), as shown in Fig. 3f (black dashed line).

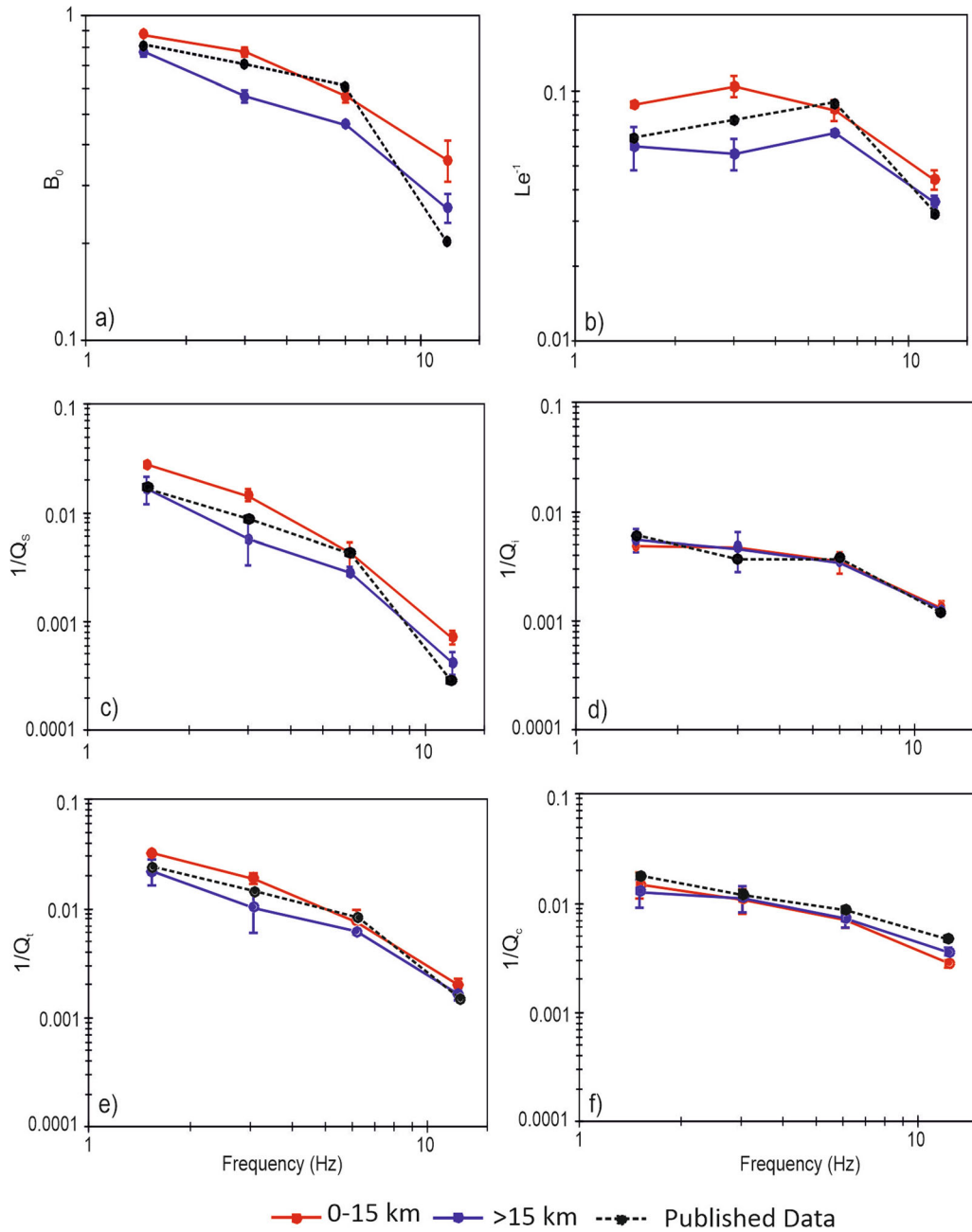


Figure 3

a, b Pattern of B_0 and Le^{-1} (and respective 1-sigma uncertainties) versus frequency, in the shallow crust (0–15 km) and lower crust/upper mantle (15–40 km) of Mt. Etna. **c–f** Pattern of Q_s^{-1} , Q_i^{-1} , Q_t^{-1} and Q_c^{-1} (and respective 1-sigma uncertainties) versus frequency, at both considered depth ranges. With black dashed line we show the pattern of Q_s^{-1} , Q_i^{-1} and Q_t^{-1} vs. frequency obtained by DP19 and that one of Q_c^{-1} obtained by Giampiccolo et al. (2021)

Table 3

Measured B_0 and Le^{-1} and corresponding Quality Factors, together with the 1-sigma uncertainties, in each sector

| Sector | N.W. | f (Hz) | B_0 | Le^{-1} | Q_i^{-1} | Q_s^{-1} | Q_t^{-1} | Q_c^{-1} |
|--------|------|--------|------------------|-------------------|---------------------|---------------------|---------------------|---------------------|
| NE | 5945 | 1.5 | 0.80 ± 0.0 | 0.064 ± 0.004 | 0.0048 ± 0.0004 | 0.0190 ± 0.0017 | 0.0238 ± 0.0021 | 0.0147 ± 0.0044 |
| | | 3 | 0.65 ± 0.0 | 0.072 ± 0.002 | 0.0047 ± 0.0 | 0.0087 ± 0.0 | 0.0134 ± 0.0 | 0.0106 ± 0.0025 |
| | | 6 | 0.50 ± 0.0 | 0.076 ± 0.0 | 0.0035 ± 0.0 | 0.0035 ± 0.0 | 0.0071 ± 0.0 | 0.0071 ± 0.0011 |
| | | 12 | 0.40 ± 0.075 | 0.048 ± 0.008 | 0.0014 ± 0.0003 | 0.0008 ± 0.0002 | 0.0022 ± 0.0005 | 0.0030 ± 0.0002 |
| NW | 3064 | 1.5 | 0.75 ± 0.0 | 0.044 ± 0.004 | 0.0041 ± 0.0006 | 0.0123 ± 0.0018 | 0.0163 ± 0.0024 | 0.0137 ± 0.0041 |
| | | 3 | 0.60 ± 0.050 | 0.056 ± 0.010 | 0.0042 ± 0.0012 | 0.0062 ± 0.0022 | 0.0104 ± 0.0034 | 0.0108 ± 0.0028 |
| | | 6 | 0.50 ± 0.025 | 0.076 ± 0.004 | 0.0035 ± 0.0029 | 0.0036 ± 0.0029 | 0.0071 ± 0.0028 | 0.0069 ± 0.0011 |
| | | 12 | 0.35 ± 0.050 | 0.040 ± 0.006 | 0.0013 ± 0.0003 | 0.0006 ± 0.0001 | 0.0019 ± 0.0004 | 0.0033 ± 0.0002 |
| SE | 3397 | 1.5 | 0.85 ± 0.0 | 0.096 ± 0.004 | 0.0053 ± 0.0003 | 0.0303 ± 0.0017 | 0.0357 ± 0.0020 | 0.0120 ± 0.0030 |
| | | 3 | 0.75 ± 0.025 | 0.112 ± 0.012 | 0.0052 ± 0.0002 | 0.0156 ± 0.0022 | 0.0208 ± 0.0024 | 0.0104 ± 0.0023 |
| | | 6 | 0.55 ± 0.050 | 0.088 ± 0.012 | 0.0037 ± 0.0009 | 0.0045 ± 0.0014 | 0.0082 ± 0.0023 | 0.0070 ± 0.0011 |
| | | 12 | 0.30 ± 0.075 | 0.036 ± 0.006 | 0.0012 ± 0.0003 | 0.0005 ± 0.0001 | 0.0017 ± 0.0004 | 0.0031 ± 0.0002 |
| SW | 3879 | 1.5 | 0.85 ± 0.0 | 0.092 ± 0.004 | 0.0051 ± 0.0003 | 0.0290 ± 0.0017 | 0.0342 ± 0.0020 | 0.0143 ± 0.0043 |
| | | 3 | 0.75 ± 0.0 | 0.100 ± 0.002 | 0.0046 ± 0.0 | 0.0139 ± 0.0 | 0.0186 ± 0.0 | 0.0100 ± 0.0024 |
| | | 6 | 0.65 ± 0.0 | 0.112 ± 0.002 | 0.0036 ± 0.0 | 0.0068 ± 0.0 | 0.0104 ± 0.0 | 0.0065 ± 0.0010 |
| | | 12 | 0.45 ± 0.050 | 0.048 ± 0.008 | 0.0012 ± 0.0005 | 0.0010 ± 0.0004 | 0.0022 ± 0.0009 | 0.0031 ± 0.0002 |

The number of waveforms used for the inversion in each sector is also reported (N.W.)

5.2. Spatial Variation of Q_i^{-1} , Q_s^{-1} and Q_c^{-1}

Thanks to a large number of earthquakes available in the depth range 0–15 km, we were able to investigate for a spatial variation of the attenuation parameters inside the whole Etna volcanic complex. We first divided the entire dataset of waveforms (16,285) into four spatial quadrants centered on the craters of Mt. Etna (15.00, 37.73; Fig. 1). On average, more than 3,000 waveforms were considered suitable for MLTWA analysis in each sector (Table 3). Then, the attenuation parameters were estimated as described in Sect. 5.1. In Table 3 we report B_0 and Le^{-1} (and the associated values of Q_i^{-1} , Q_s^{-1} , and Q_t^{-1}) for each sector, whereas, in Fig. 4 we show the pattern of Q_t^{-1} , Q_i^{-1} , and Q_s^{-1} vs. frequency. Such a comparison shows few but remarkable results.

Overall, the estimates of the attenuation parameters calculated with MLTWA show that the intrinsic attenuation is similar for the four sectors, while the scattering attenuation shows some differences among them. In particular, both southern sectors (SW and SE) seem to be more heterogeneous than the northern

ones, at least at frequencies lower than 6 Hz (Fig. 4; Table 3). In Table 3 we also report the Q_c^{-1} values obtained in each sector and frequency. Plots showing the pattern of Q_c^{-1} , Q_i^{-1} , Q_s^{-1} , and Q_t^{-1} versus frequency in all sectors investigated are shown in Fig. 4. It is remarkable that no differences in the seismic coda wave attenuation are observed and the Q_c^{-1} values in each sector are comparable with the mean Q_c^{-1} estimate obtained by Giampiccolo et al. (2021).

A more in-depth investigation into a possible depth dependence of scattering attenuation in each sector was ultimately performed (Fig. 5; Tables S3, S4). However, due to the fact that the seismicity is not uniformly distributed in depth, a low number of earthquakes is available for the depth range between 15 and 40 km in the eastern flank of the volcano (NE and SE; see Table S2 in Supplementary Material). Thus, the separate inversion of the earthquake waveforms for the whole eastern flank led to high uncertainties for the 15–40 km group of earthquakes (Table S2; Fig. 5b). However, the comparison among the Q_s^{-1} patterns vs. frequency in each sector (Fig. 5)

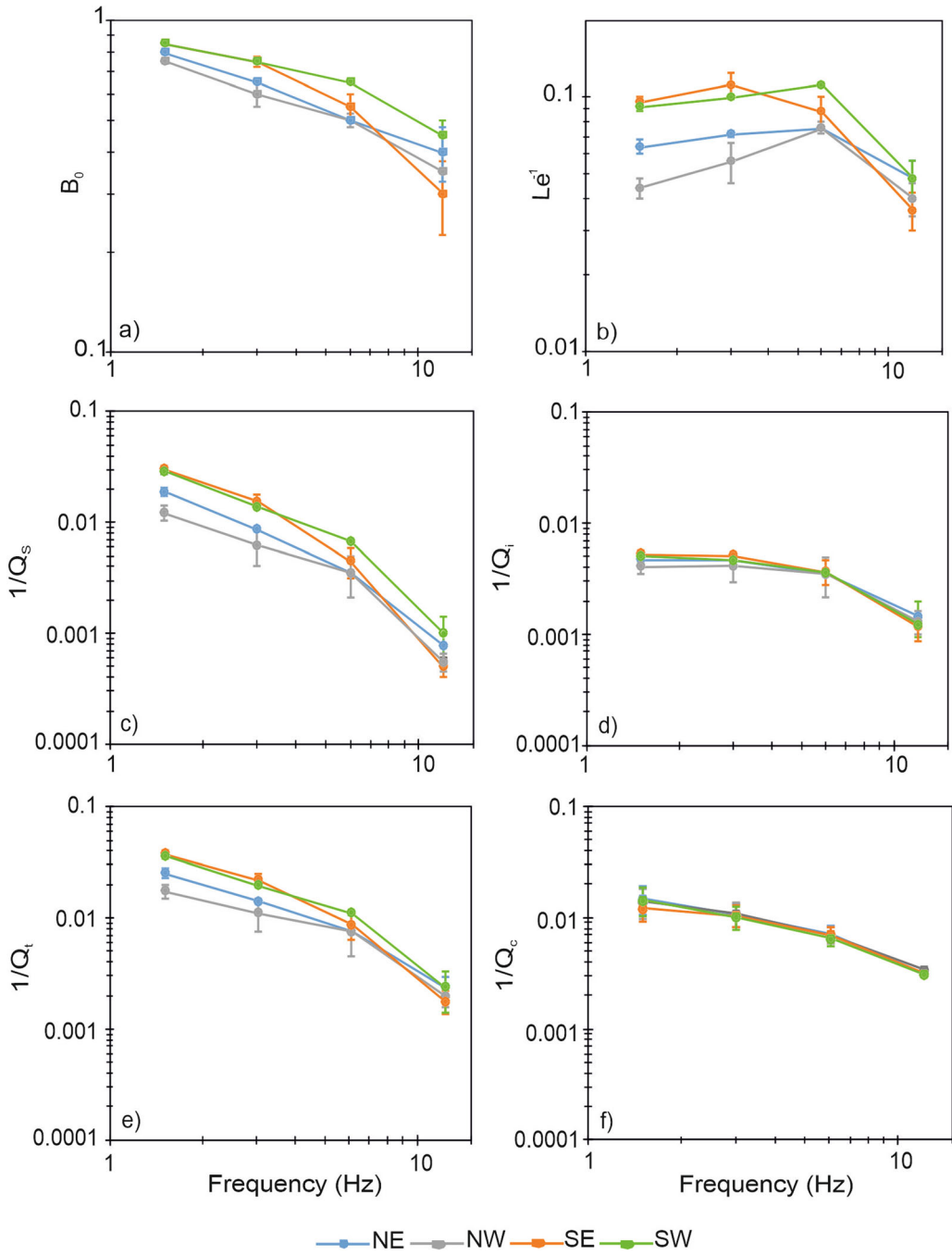


Figure 4

a, b Pattern of B_0 and Le^{-1} (**a** and **b**) and of Q_s^{-1} , Q_i^{-1} , Q_t^{-1} , and Q_c^{-1} (**c-f**) versus frequency for the four Mt. Etna sectors analyzed. Respective 1-sigma uncertainties for each estimate are also reported. Different colors indicate the zones, as shown in the legend

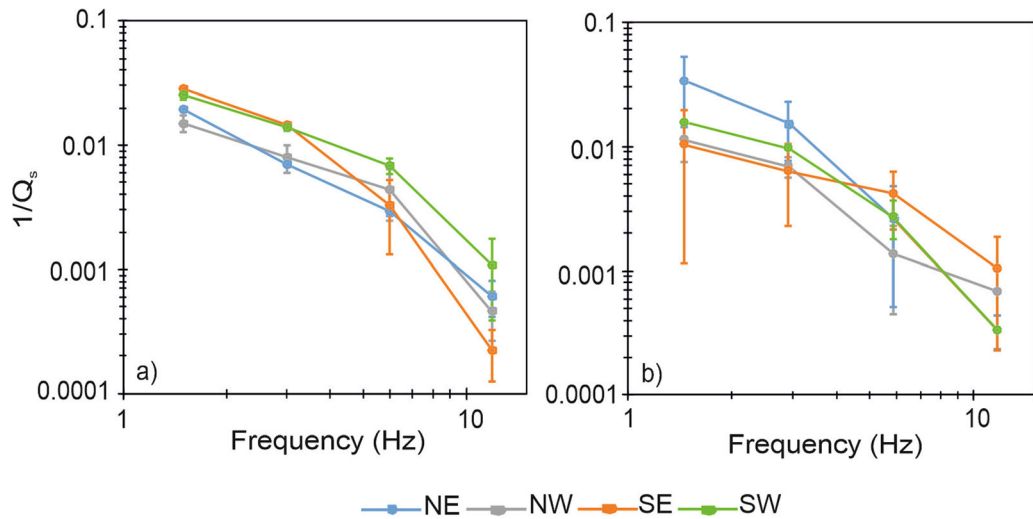


Figure 5

Pattern of Q_s^{-1} versus frequency for the four sectors Mt. Etna analyzed, in the 0–15 km (a) and 15–40 km (b) depth ranges. Respective 1-sigma uncertainties for each estimate are also reported

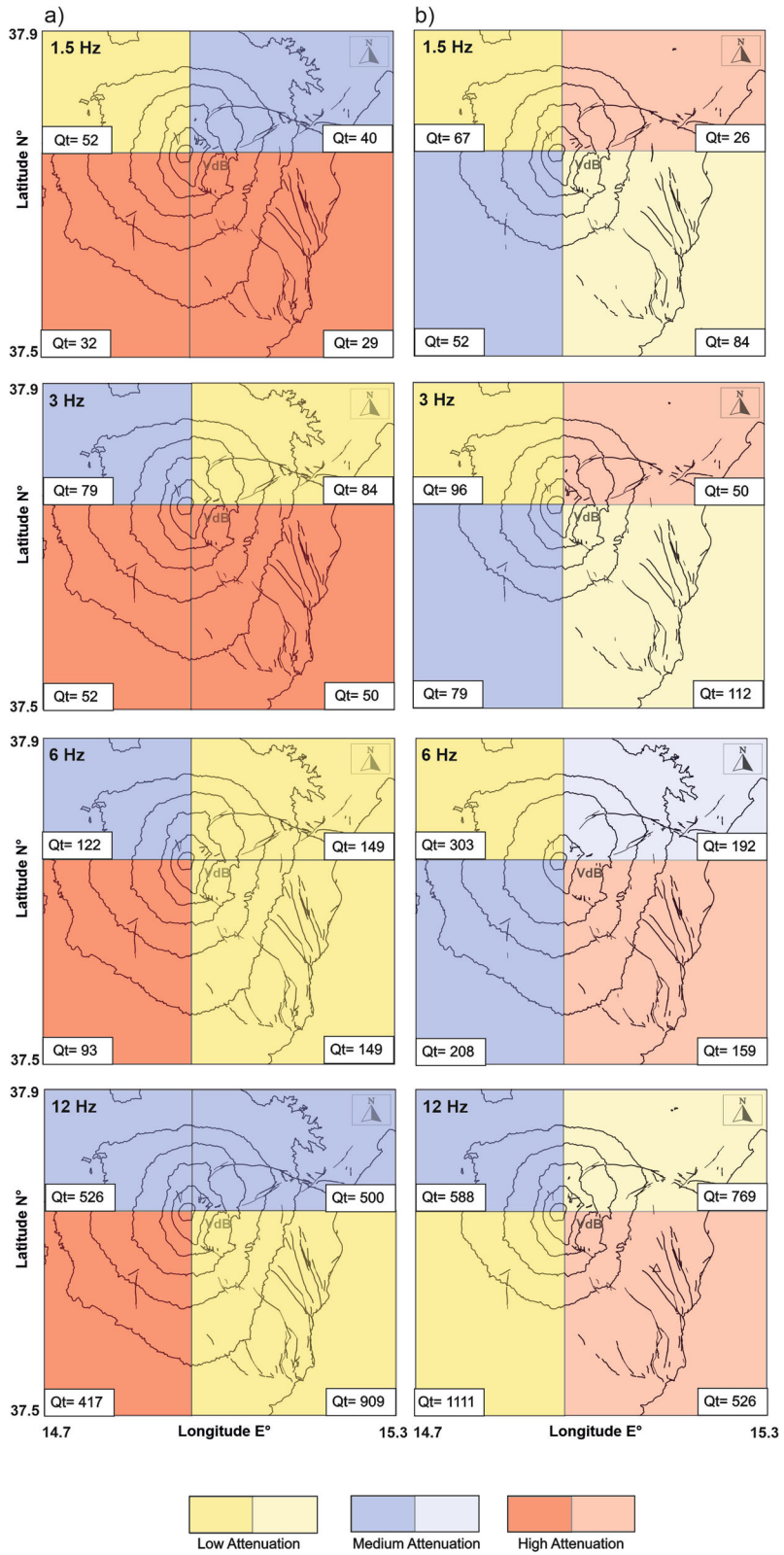
further confirms that in the depth range 0–15 km, scattering is higher at low frequencies for the two southern sectors (below 6 Hz in the SE sector and below 12 Hz in the SW one) with estimates significantly outside the respective error bars at 1-sigma (see also Figs. S1 and S2 in Supplementary Material). In Fig. 6 we report a summary sketch map showing the main total attenuation differences (Q_t) in the two depth ranges analyzed and within the four sectors around Mt. Etna.

6. Discussion and Conclusions

Separate estimates of the intrinsic and scattering attenuation (Q_i^{-1} and Q_s^{-1}) by applying MLTWA under the simple assumption of constant velocity in half space show that the intrinsic attenuation at Mt. Etna is fairly uniform across four sectors in which the whole volcanic complex of Mt. Etna is divided (Fig. 1) and does not vary with depth. However, some differences can be observed in the distribution of scattering attenuation. The first evidence is that the scattering coefficient in the shallow crust is greater

than that measured in the lower crust/upper mantle (Table 2; Fig. 3). This indicates that the geological heterogeneity characterizing the shallow crust of Etna (magmatic intrusions, multiple fracture systems oriented in different directions, velocity, and density fluctuations, strong stratification, etc.) play an important role in the redistribution of the seismic energy lost by the primary waves in the seismic coda.

The predominance of scattering attenuation in the crust of Etna has been clearly highlighted in recent studies (Del Pezzo et al., 2019; Ibáñez et al., 2019) and is in good agreement with the numerous results from 3D velocity and attenuation images performed in the area, showing the presence of velocity contrasts (both P and S waves) and attenuation anomalies in the upper crust (Alparone et al., 2012; Barberi et al., 2004; De Gori et al., 2005, 2011; Díaz-Moreno et al., 2018; Giampiccolo et al., 2020, 2021; Ibáñez et al., 2019; Martínez-Arevalo et al., 2005; Patanè et al., 2002, 2006). Comparable results have been obtained in other volcanoes, such as Mount Merapi (Wegler & Luhr, 2001) and Vesuvius (Bianco et al., 1999; Del Pezzo et al., 2016).



◀Figure 6

Plot showing the main attenuation differences (Q_i) at each frequency, within the four sectors around Mt. Etna and in the two depth ranges: **a** 0–15 km; **b** 15–40 km. Lighter colors in **b** indicate that the attenuation characteristics are not statistically significant, due to high uncertainties associated with the Q estimates

Another important evidence that emerges from the present study is the variation in the scattering attenuation observed below 6 Hz among the sectors into which the Etna area was divided (Table 3; Fig. 4). The contrasts are statistically significant, as they go beyond uncertainties and suggest variability in the rock properties characterizing the four sectors, evidenced by the longer wavelength propagation. A drawback of this interpretation could be the greater dispersion of the experimental points around the theoretical best-fit curve at low frequency (Fig. 2). This major dispersion, however, has been explained (see e.g. Sato et al., 2012) as due to radiation pattern effects which are stronger at low frequency. Assuming that the “diffusion regime” is reached at Mt. Etna, Scattering Mean Free Path should be greater than the wavelength (Del Pezzo & Ibáñez, 2020). At the frequency of 3 Hz, λ is of the order of 1 km and the Mean Free Path (the inverse of the scattering coefficient) is of the order of 15 km. It is noteworthy that the dimensions of most of the structural elements (Fig. 1) in the Southern Flanks of Mt. Etna (of the order of 2 km; e.g. Giampiccolo et al., 2020) are of the same order of the lowest frequency investigated, confirming the Diffusion regime and the geological interpretation of the scattering phenomena. Above 6 Hz the differences between the parameters estimated in each sector fall within the estimated uncertainties (Table S3; Fig. 5; Fig S1).

Uniformity in seismic attenuation at high frequencies is also clearly evident from the MLTWA results at different depths (Table 2; Fig. 3). It should be noted that MLTWA provides a spatial average of different attenuation parameters over the volume under study; therefore, the uniformity observed between sectors at high frequencies must be interpreted as uniformity between the “averages” calculated for each sector. In other words, the crustal volumes showing spatial variations of Etna’s attenuation parameters, if any, are much smaller than the

extent of the four quadrants used. As a last step, we improved information about the attenuation of coda waves (Q -coda) achieved in the same area by Giampiccolo et al. (2021) using a more limited data set. Our results are in good agreement with those estimated previously, indicating the robustness of the Q -coda estimates and verifying the stability of the Q_c images shown by Giampiccolo et al. (2021).

The Q_c^{-1} values were compared with Q_i^{-1} , Q_s^{-1} Q_t^{-1} estimates. It is noteworthy, similar Q_c^{-1} values were found for data in the two examined focal depth ranges (Table 2; Fig. 7) and in all 4 sectors (Table 3; Fig. 7). Q_c^{-1} results were found to be closer to total attenuation (Fig. 7a-d), in agreement with many similar observations reported in the literature (e.g., Akinci & Eyidogan, 2000; Bianco et al., 2005; Mayeda et al., 1992; Pujades et al., 1997). Q_c is a parameter with a controversial physical meaning, as it is calculated assuming a Single Scattering regime, which is almost never present. It has been demonstrated that, when Q_c is calculated for long lapse times (in the “equipartition” regime, Margerin et al., 1998) it approaches Q_i . The differences between the present estimates of Q_c and Q_i may indicate that the equipartition regime is not reached in the first 45 s of the analyzed signal. However, in the whole southern flank, below 6 Hz, Q_c^{-1} is almost halfway between Q_t^{-1} and Q_i^{-1} (Fig. 7e, f). This result can be explained by the significant heterogeneity (i.e., Margerin et al., 1998) characterizing the southern sector of the volcano, which results in approximate energy equipartition at early lapse times.

The present research provides new details in the knowledge of the attenuation characteristics of Mt. Etna, both in the shallow crust and in the lower crust/upper mantle. Moreover, the presented results confirm the previously observed correlation between seismic wave attenuation and the tectonic complexity of the crust in the study region. Furthermore, the results suggest that a 3D inversion of the attenuation parameters estimated on the single source-receiver paths and based on proper scattering kernels, is necessary, in order to construct a detailed image of the spatial distribution of the seismic attenuation in the broader Etna area.

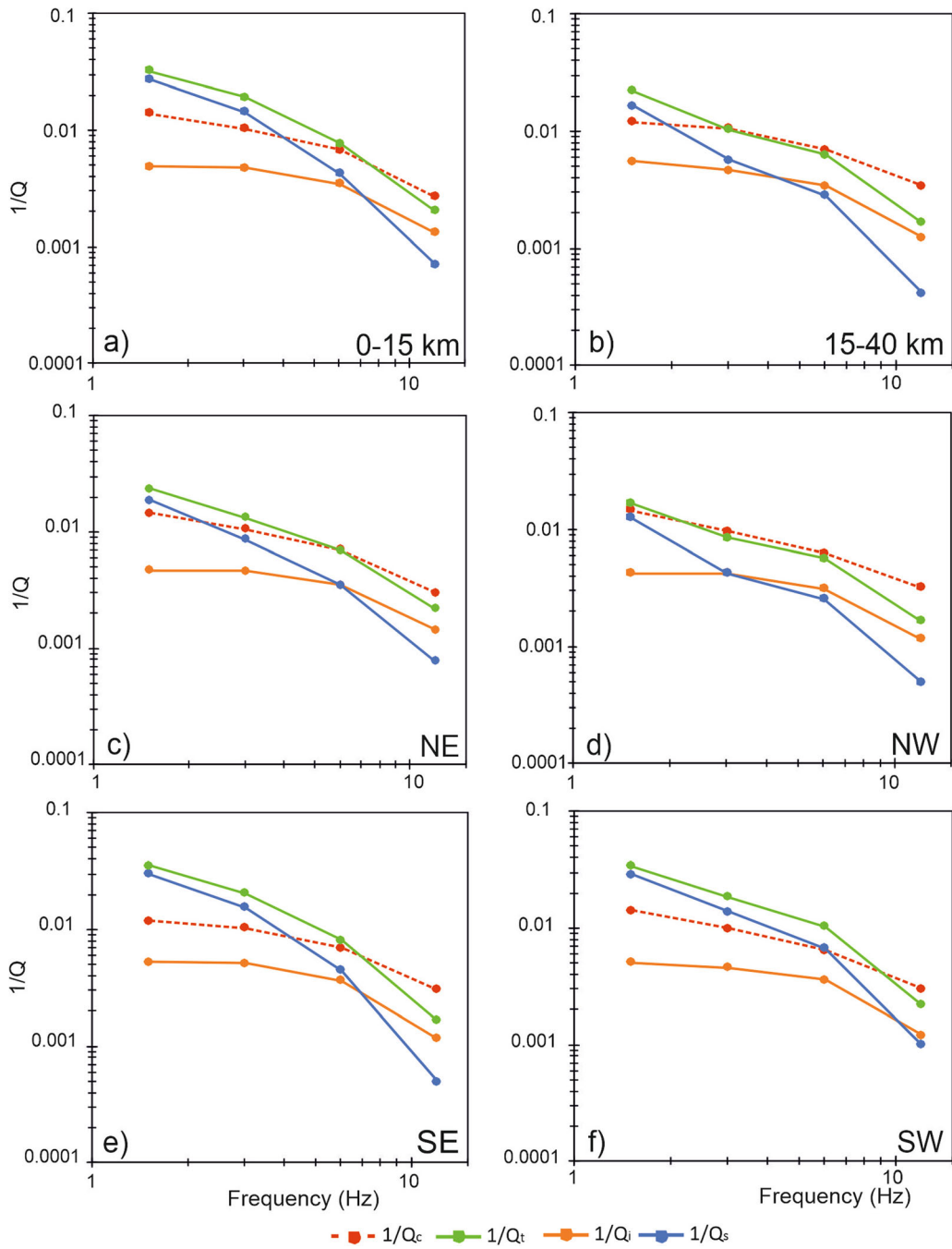


Figure 7

Pattern of Q_s^{-1} , Q_t^{-1} , Q_i^{-1} , and Q_c^{-1} versus frequency for the two depth ranges and the four Mt. Etna sectors investigated (see Fig. 1)

Acknowledgements

We wish to thank the INGV-OE seismic technical staff who ensure the regular working of the seismic monitoring network. We are grateful to Giuseppe Di Grazia for his help during the data preparation process. Finally, we thank the Editor and both reviewers for their constructive comments and suggestions. This research was carried out in the frame of the IMPACT PROJECT (INGV Department strategic Projects—2019) WP1, Task 2-Mt. Etna structure.

Author Contributions All authors contributed to the study conception and design. Material preparation, data collection and analysis were performed by Elisabetta Giampiccolo, Tiziana Tuvè and Edoardo Del Pezzo. The first draft of the manuscript was written by Elisabetta Giampiccolo and all authors commented on previous versions of the manuscript. All authors have read and approved the final manuscript.

Funding

This research was carried out in the frame of the IMPACT PROJECT (INGV Department strategic Projects—2019) WP1, Task 2-Mt. Etna structure.

Data availability

Seismic waveforms can be retrieved in the EIDA database, <https://www.orfeus-eu.org/data/eida/>. Data are available from authors.

Declarations

Conflict of interest The authors have no relevant financial or non-financial interests to disclose.

Open Access This article is licensed under a Creative Commons Attribution 4.0 International License, which permits use, sharing, adaptation, distribution and reproduction in any medium or format, as long as you give appropriate credit to the original author(s) and the source, provide a link to the Creative Commons licence, and indicate if changes were made. The images or other third party material in this article are included in the article's Creative Commons licence, unless indicated otherwise in a credit line to the material. If material is not included in the article's Creative Commons licence and your intended use is not permitted by statutory regulation or exceeds the permitted use, you will need to obtain permission directly from the copyright holder. To view a copy of this licence, visit <http://creativecommons.org/licenses/by/4.0/>.

Publisher's Note Springer Nature remains neutral with regard to jurisdictional claims in published maps and institutional affiliations.

REFERENCES

- Aki, K. (1980). Scattering and attenuation of shear waves in the lithosphere. *Journal of Geophysical Research: Solid Earth*, 85(B11), 6496–6504. <https://doi.org/10.1029/JB085iB11p06496>
- Aki, K., & Chouet, B. (1975). Origin of coda waves: Source, attenuation and scattering effects. *Journal of Geophysical Research*, 80, 3322–3342.
- Akinci, A., Del Pezzo, E., & Malagnini, L. (2020). Intrinsic and scattering seismic wave attenuation in the Central Apennines (Italy). *Physics of the Earth and Planetary Interiors*, 303, 106498.
- Akinci, A., & Eyidogan, H. (2000). Scattering and anelastic attenuation of seismic energy in the vicinity of north Anatolian fault zone, eastern Turkey. *Physics of the Earth and Planetary Interiors*, 122, 229–239.
- Alparone, S.C., Maiolino, V., Mostaccio, A., Scaltrito, A., Ursino, A., Barberi, G., Di Grazia, G., Giampiccolo, E., Musumeci, C., Scarfi, L., & Zuccarello, L. (2015). Mt. Etna Seismic Catalog 2000–2010. Istituto Nazionale di Geofisica e Vulcanologia (INGV) – Osservatorio Etneo, from https://doi.org/10.13127/etnasc/2000_2010
- Alparone, S., Barberi, G., Di Grazia, G., Giampiccolo, E., Maiolino, V., Mostaccio, A., Musumeci, C., Scaltrito, A., Tuvè, T., & Ursino, A. (2020a). *Mt. Etna Seismic Catalog 2014–2016 (Version 1)*. Istituto Nazionale di Geofisica e Vulcanologia (INGV). https://doi.org/10.13127/ETNASC/2014_2016
- Alparone, S. C., Barberi, G., Di Grazia, G., Giampiccolo, E., Maiolino, V., Mostaccio, A., Musumeci, C., Scaltrito, A., & Ursino, A. (2020b). *Mt. Etna Seismic Catalog 2011–2013 (Version 1)*. Istituto Nazionale di Geofisica e Vulcanologia (INGV). https://doi.org/10.13127/ETNASC/2011_2013
- Alparone, S. C., Barberi, G., Di Grazia, G., Giampiccolo, E., Maiolino, V., Mostaccio, A., Musumeci, C., Scaltrito, A., Tuvè, T., & Ursino, A. (2022). *Mt. Etna Seismic Catalog 2017–2019 (Version 1)*. Istituto Nazionale di Geofisica e Vulcanologia (INGV). https://doi.org/10.13127/ETNASC/2017_2019
- Alparone, S. C., Barberi, G., Cocina, O., Giampiccolo, E., Musumeci, C., & Patanè, D. (2012). Intrusive mechanism of the 2008–2009 Mt. Etna eruption: Constraints by tomographic images and stress tensor analysis. *Journal of Volcanology and Geothermal Research*, 229, 50–63. <https://doi.org/10.1016/j.jvolgeores.2012.04.001>
- Alparone, S. C., Cocina, O., Gambino, S., Mostaccio, A., Spampinato, S., Tuvè, T., & Ursino, A. (2013). Seismological features of the Pernicana-Provenzana Fault System (Mt. Etna, Italy) and implications for the dynamics of northeastern flank of the volcano. *Journal of Volcanology and Geothermal Research*, 118, 1–11.
- Azzaro, R., Branca, S., Gwinner, K., & Coltelli, M. (2012). The volcano-tectonic map of Etna volcano, 1:100.000 scale: An integrated approach based on a morphotectonic analysis from high-resolution DEM constrained by geologic, active faulting

- and seismotectonic data. *Italian Journal of Geosciences*, 131(1), 153–170. <https://doi.org/10.3301/IJG.2011.29>
- Azzaro, R., D'Amico, S., Peruzza, L., & Tuvè, T. (2013). Probabilistic seismic hazard at Mt. Etna (Italy): the contribution of local fault activity in mid-term assessment. *Journal of Volcanology and Geothermal Research*, 251, 158–169. In special issue: flank instability at Mt. Etna, Acocella V, Puglisi P, Amelung F (Eds).
- Badi, G., Del Pezzo, E., Ibáñez, J. M., Bianco, F., Sabbione, N., & Araujo, M. (2009). Depth dependent seismic scattering attenuation in the Nuevo Cuyo region (southerncentral Andes). *Geophysical Research Letters*, 36(24), L24307. <https://doi.org/10.1029/2009GL041081>
- Barberi, G., Cosentino, M. T., Gervasi, A., Guerra, I., Neri, G., & Orecchio, B. (2004). Crustal seismic tomography in the Calabrian Arc region, south Italy. *Physics of the Earth and Planetary Interiors*, 147, 297–314.
- Barberi, G., Di Grazia, G., Ferrari, F., Giampiccolo, E., Maiolino, V., Mostaccio, A., Musumeci, C., Scaltrito, A., Sciotto, M., Tusa, G., Tuvè, T., & Ursino, A. (2020). *Mt. Etna Revised Seismic Catalog from 2020 (EtnaRSC2020) (Version 1)*. Istituto Nazionale di Geofisica e Vulcanologia (INGV). <https://doi.org/10.13127/ETNASC/ETNASC2020>
- Bianco, F., Castellano, M., Del Pezzo, E., & Ibanez, J. M. (1999). Attenuation of short period seismic waves at Mt. Vesuvius, Italy. *Geophysical Journal International*, 138(1), 67–76.
- Bianco, F., Del Pezzo, E., Castellano, M., Ibanez, J., & Di Luccio, F. (2002). Separation of intrinsic and scattering seismic attenuation in the Southern Apennine zone, Italy. *Geophysical Journal International*, 150, 10–22.
- Bianco, F., Del Pezzo, E., Malagnini, L., Di Luccio, F., & Akinci, A. (2005). Separation of depth-dependent intrinsic and scattering seismic attenuation in the northeastern sector of the Italian Peninsula. *Geophysical Journal International*, 161, 130–142.
- Bousquet, J. C., & Lanzafame, G. (2004). The tectonics and geodynamics of Mt. Etna: Synthesis and interpretation of geological and geophysical data. In A. Bonaccorso, S. Calvari, M. Coltelli, C. Del Negro, & S. Falsaperla, (Eds.), *The Mt. Etna volcano* (pp. 29–47). Washington, DC: AGU.
- Branca, S., Coltelli, M., De Beni, E., & Wijbrans, J. (2008). Geological evolution of Mount Etna volcano (Italy) from earliest products until the first central volcanism (between 500 and 100 ka ago) inferred from geochronological and stratigraphic data. *International Journal of Earth Sciences*, 97, 135–152.
- Castro-Melgar, I., Prudencio, J., Cannata, A., Del Pezzo, E., & Ibáñez, J. M. (2021). Small-scale volcanic structures of the Aeolian volcanic arc revealed by seismic attenuation. *Frontiers in Earth Science*, 9, 725402. <https://doi.org/10.3389/feart.2021.725402>
- De Gori, P., Chiarabba, C., Giampiccolo, E., Martinez-Arevalo, C., & Patané, D. (2011). Body wave attenuation heralds incoming eruptions at Mt. Etna. *Geology*, 39, 503–506.
- De Gori, P., Chiarabba, C., & Patané, D. (2005). Qp structure of Mount Etna: Constraints for the physics of the plumbing system. *Journal of Geophysical Research*, 110, B05303. <https://doi.org/10.1029/2003JB002875>
- de Lorenzo, S., Filippucci, M., Giampiccolo, E., & Patané, D. (2006). Intrinsic Qp at Mt. Etna from the inversion of rise times of 2002 microearthquake sequence. *Annals of Geophysics*, 49(6), 1215–1234.
- Del Pezzo, E., Bianco, F., Giampiccolo, E., Tusa, G., & Tuvè, T. (2015). A reappraisal of seismic Q evaluated at Mt. Etna volcano. Receipt for the application to risk analysis. *Journal of Seismology*, 19(1), 105–119.
- Del Pezzo, E. (2008). Earth heterogeneity and scattering effects of seismic waves: Seismic wave scattering in volcanoes. *Advances in Geophysics*, 50, 353–371.
- Del Pezzo, E., & Bianco, F. (2010). Two-layer earth model corrections to the MLTWA estimates of intrinsic- and scattering-attenuation obtained in a uniform half-space. *Geophysical Journal International*, 182(2), 949–955.
- Del Pezzo, E., Bianco, F., Marzorati, S., Augliera, P., D'Alema, E., & Massa, M. (2011). Depth-dependent intrinsic and scattering seismic attenuation in north central Italy. *Geophysical Journal International*, 186(1), 373–381.
- Del Pezzo, E., Giampiccolo, E., Tuvè, T., Di Grazia, G., Gresta, S., & Ibáñez, J. M. (2019). Study of the regional pattern of intrinsic and scattering seismic attenuation in Eastern Sicily (Italy) from local earthquakes. *Geophysical Journal International*, 218, 1456–1468. <https://doi.org/10.1093/gji/ggz208>
- Del Pezzo, E., & Ibáñez, J. M. (2020). Seismic coda-waves imaging based on sensitivity kernels calculated using an heuristic approach. *Geosciences*, 10, 304.
- Del Pezzo, E., Ibáñez, J., Morales, J., Akinci, A., & Maresca, R. (1995). Measurements of intrinsic and scattering seismic attenuation in the crust. *Bulletin of the Seismological Society of America*, 85, 1373–1380.
- Del Pezzo, E., Ibáñez, J., Prudencio, J., Bianco, F., & De Siena, L. (2016). Absorption and scattering 2D volcano images from numerically calculated space-weighting functions. *Geophysical Journal International*, 206, 742–756.
- Diaz-Moreno, A., Barberi, G., Cocina, O., Koulakov, I., Scarfi, L., Zuccarello, L., Prudencio, J., Garcia-Yeguas, A., Alvarez, I., Garcia, L., & Ibanez, J. M. (2018). New insights on Mt. Etna's Crust and relationship with the regional tectonic framework from joint active and passive P-Wave seismic tomography. *Surveys in Geophysics*, 39(1), 57–97. <https://doi.org/10.1007/s10712-017-9425-3>
- Fehler, M., Hoshiya, M., Sato, H., & Obara, K. (1992). Separation of scattering and intrinsic attenuation for the Kanto-Tokai Region, Japan, using measurements of S-wave energy versus hypocentral distance. *Geophysical Journal International*, 108(3), 787–800.
- Gabrielli, S., Akinci, A., Napolitano, F., Del Pezzo, E., & De Siena, L. (2022). 3D scattering and absorption model during the 2016–2017 Central Italy seismic sequence. In *EGU General Assembly 2022*, Vienna, Austria, 23–27 May 2022, EGU22-7998. 10.5194/egusphere-egu22-7998.
- Giampiccolo, E., D'Amico, S., Patané, D., & Gresta, S. (2007). Attenuation and source parameters of shallow microearthquakes at Mt. Etna volcano, Italy. *Bulletin of the Seismological Society of America*, 97(1B), 184–197. <https://doi.org/10.1785/0120050252>
- Giampiccolo, E., Cocina, O., De Gori, P., & Chiarabba, C. (2020). Dyke intrusion and stress-induced collapse of volcano flanks: The example of the 2018 event at Mt. Etna (Sicily, Italy). *Nature Research - Scientific Reports*, 10, 6373. <https://doi.org/10.1038/s41598-020-63371-3>
- Giampiccolo, E., Del Pezzo, E., Tuvè, T., Di Grazia, G., & Ibáñez, J. M. (2021). 3-D Q-coda attenuation structure at Mt Etna (Italy).

- Geophysical Journal International*, 227, 544–558. <https://doi.org/10.1093/gji/ggab235>
- Giampiccolo, E., & Tuve, T. (2018). Regionalization and dependence of coda-Q on frequency and lapse time in the seismically active Peloritani region (northeastern Sicily, Italy). *Journal of Seismology*, 22(4), 1059–1074.
- De Gori, P., Giampiccolo, E., Cocina, O., Branca, S., Doglioni, C., & Chiarabba, C. (2021). Re-pressurized magma at Mt. Etna, Italy, may feed eruptions for years. *Communications Earth & Environment*, 2, 216. <https://doi.org/10.1038/s43247-021-00282-9>
- Hoshiba, M., Rietbrock, A., Scherbaum, F., Nakahara, H., & Haberland, C. (2001). Scattering attenuation and intrinsic absorption using uniform and depth dependent model—Application to full seismogram envelope recorded in Northern Chile. *Journal of Seismology*, 5, 157–179.
- Ibáñez, J. M., Castro-Melgar, I., Cocina, O., Zuccarello, L., Branca, S., Del Pezzo, E., & Prudencio, J. (2019). First 2-D intrinsic and scattering attenuation images of Mt. Etna volcano and surrounding region from active seismic data. *Geophysical Journal International*, 220(1), 267–277. <https://doi.org/10.1093/gji/ggz450>
- Lentini, F. (1982). The geology of the Etna basement. *Memorie Della Società Geologica Italiana*, 23, 7–25.
- Lo Giudice, E., & Rasà, R. (1992). Very shallow earthquakes and brittle deformation in active volcanic areas: The Etnean region as example. *Tectonophysics*, 202, 257–268.
- Margerin, L., Campillo, M., & van Tiggelen, B. (1998). Radiative transfer and diffusion of waves in a layered medium: New insight into coda Q. *Geophysical Journal International*, 134(2), 596–612. <https://doi.org/10.1111/j.1365-246X.1998.tb07142.x>
- Martinez-Arevalo, C., Patanè, D., Rietbrock, A., & Ibanez, J. M. (2005). The intrusive process leading to the Mt. Etna 2001 flank eruption: constraints from 3-D attenuation tomography. *Geophysical Research Letters*, 32, L21309. <https://doi.org/10.1029/2005GL023736>
- Mayeda, K., Koyanagi, S., Hoshiba, M., Aki, K., & Zeng, Y. (1992). A comparative study of scattering, intrinsic, and coda Q–1 for Hawaii, Long Valley and central California between 1.5 and 15 Hz. *Journal of Geophysical Research*, 97, 6643–6659.
- Mayor, J., Calvet, M., Margerin, L., & Vanderhaeghe, O. (2016). Crustal structure of the Alps as seen by attenuation tomography. *Earth and Planetary Science Letters*, 439, 71–80.
- Monaco, C., De Guidi, G., & Ferlito, C. (2010). The morphotectonic map of Mt. Etna. *Bollettino Della Società Geologica Italiana*, 129(3), 408–428.
- Monaco, C., Tapponnier, P., Tortrici, L., & Gillot, P. Y. (1997). Late Quaternary slip rates on the Acireale-Piedimonte normal faults and tectonic origin of Mt. Etna (Sicily). *Earth and Planetary Science Letters*, 147, 125–139.
- Paasschens, J. (1997). Solution of the time-dependent Boltzmann equation. *Physical Review*, 56, 1135–1141.
- Patanè, G., Ferrucci, F., & Gresta, S. (1994). Spectral features of microearthquakes in volcanic areas: Attenuation in the crust and amplitude response of the site at Mt. Etna, Italy. *Bulletin of the Seismological Society of America*, 84(6), 1842–1860.
- Patanè, D., Chiarabba, C., Cocina, O., De Gori, P., Moretti, M., & Boschi, E. (2002). Tomographic images and 3D earthquake locations of the seismic swarm preceding the 2001 Mt. Etna eruption: Evidence for a dyke intrusion. *Geophysical Research Letters*, 29(10), 1497.
- Patanè, D., Cocina, O., Falsaperla, S., Privitera, E., & Spampinato, S. (2004). Mt. Etna volcano: A seismological frame work. In S. Calvari, A. Bonaccorso, M. Coltelli, C. Del Negro, & S. Falsaperla (Eds.), *The Mt. Etna volcano* (pp. 147–165). Washington, DC: AGU.
- Patanè, D., Barberi, G., Cocina, O., De Gori, P., & Chiarabba, C. (2006). Time-resolved seismic tomography detects magma intrusions at Mount Etna. *Science*, 313, 821–823.
- Pujades, L. G., Ugalde, A., Canas, J. A., Navarro, M., Badal, F. J., & Corchete, V. (1997). Intrinsic and scattering attenuation from observed seismic codas in the Almeria Basin (southeastern Iberian Peninsula). *Geophysical Journal International*, 129, 281–291.
- Sato, H. (1977). Energy propagation including scattering effects: Single isotropic scattering approximation. *Journal of Physics of the Earth*, 25, 27–41.
- Sato, H., Fehler, M. C., & Maeda, T. (2012). Introduction. In *Seismic wave propagation and scattering in the heterogeneous Earth: Second edition*. Berlin: Springer. https://doi.org/10.1007/978-3-642-23029-5_1
- Sicali, S., Barbano, M. S., D’Amico, S., & Azzaro, R. (2014). Characterization of seismicity at Mt. Etna volcano (Italy) by inter-event time distribution. *Journal of Volcanology and Geothermal Research*, 270, 1–9.
- Singh, C., Biswas, R., Sriyayanthi, G., & Ravi Kumar, M. (2017). Relative role of intrinsic and scattering attenuation beneath the Andaman Islands, India and tectonic implications. *Physics of the Earth and Planetary Interiors*, 271, 19–28.
- van Lateen, M., Eulenfeld, T., & Wegler, U. (2021). Comparison of Multiple Lapse Time Window Analysis and Qopen to determine intrinsic and scattering attenuation. *Geophysical Journal International*, 228(2), 913–926.
- Wegler, U., & Luhr, B. G. (2001). Scattering behaviour at Merapi volcano (Java) revealed from an active seismic experiment. *Geophysical Journal International*, 145, 579–592.
- Wolfram Research, Inc. (2022). *Mathematica, Version 13.2*. Champaign, IL.
- Zeng, Y. (1991). Compact solutions for multiple scattered wave energy in time domain. *Bulletin of the Seismological Society of America*, 81, 1022–1029.